Enhancement of finger motion range with compliant anthropomorphic joint design

Utku Çulha[1, 2] and Fumiya Iida[2]

[1] Department of Mechanical and Process Engineering, ETH Zurich, Switzerland

[2] Biologically Inspired Robotics Laboratory, University of Cambridge, United Kingdom

E-mail: utku.culha@mavt.ethz.ch

Abstract. Robotic researchers have been greatly inspired from the human hand in the search of designing and building adaptive robotic hands. Especially, joints have received a lot of attention upon their role in maintaining the passive compliance that gives the fingers flexibility and extendible motion ranges. Passive compliance, which is the tendency to be employed in motion under the influence of an external force, is the result of the stiffness and the geometrical constraints of the joints that define the direction of the motion. Based on its building elements, human finger joints have multi-directional passive compliance which means that they can move in multiple axis of motion under external force. However, due to their complex anatomy, only simplified biomechanical designs based on physiological analysis are preferred up to day in robotics. To imitate the human joints, these designs either use fixed degree of freedom mechanisms which substantially limit the motion axes of compliance or soft materials that can deform in many directions but hinder fingers' force exertion capacities. In order to find a solution that lies between these two design approaches, we are using anatomically correct finger bones, elastic ligaments and antagonistic tendons to build anthropomorphic joints with multi-directional passive compliance and strong force exertion capabilities. We use interactions between an index finger and a thumb to show that our joints allow the extension of the range of motion of the fingers up to 245% and gripping size to 63% which can be beneficial for mechanical adaptation in gripping larger objects.

1. Introduction

Human hand has always been an inspiration for robotic researchers for its manipulation capacity [1] and bond with intelligent life [2]. Being able to adapt to different size and shape of objects, squeeze in compact volumes in constrained environments and use tools for a great range of purposes are just some impressive functions of the human hand. Therefore, researchers have been working on developing human like robotic hands in order to replicate such functions for robotic tasks [3]. However, building a complete replica of the human hand is still very challenging because of the complexity of tissue anatomies and how they are put together in a confined space. Also, features such as having more than 25 degrees of freedom (DOF), lightweight design, antagonistic tendon and muscle actuation, highly distributed tactile sensing and passive compliant joints that yield flexibility are additional challenges for robotic hands. That is why, the wide range of robotic hands employ only a part of these features instead of attempting to achieve all of them at the same time [4].

One of the most interesting features of the hand is the complex structure of its joints and its effect on passive compliance. Passive compliance, which is the tendency to be employed in motion under the influence of an external force originating from the environment, is the result of the stiffness and the geometry of the joints. These two combined, dictate the constraints on the joints and define fingers' direction of motion as a result of external forces. Depending on these, passive compliancy of the joints can have either fixed degree of freedom or be multi-directional. Due to its elastic elements such as ligaments and tendons, synovial fluid and the geometry of the bone cavity [5], human finger joints have multi-directional compliance which constitutes the hand's physical adaptivity property. Conforming to the shapes of unprecedented objects, elastically deforming in small volumes and resisting impact stimuli demonstrate human hand's adaptation capacity which can be observed during interactions with objects and the environment.

Under the guidance of physiological investigation of human hand [5], robotics researchers have developed basically two different approaches in producing anthropomorphic joints as shown in Figure 1. First approach employs simplified mechanical representations of the joints with limited DOF mechanisms such as hinge, gimbal and ball joints. Stanford/JPL [6], Barrett [7], Gifu [8], Robonaut [9], Utah/MIT [10], DLR [11], Shadow [12] and ACT [13] hands are successful examples for robotic hands which use fixed DOF mechanisms to replicate the joint kinematics of the human hand. While these hands can make use of inverse kinematics to provide precise position control and produce strong forces at finger tips due to rigid limb structure, their passive compliance is either non-existent or highly constrained to a fixed axis of motion because of their joint mechanisms. Therefore, in order to demonstrate adaptivity during interaction, these hand designs rely on either active impedance control to constantly monitor the force they exert, or position control to move their fingers to postures where passive elements can be effective in allowed, constrained directions. Achieving compliance in these ways does not only require more complicated controller regimes but also prior knowledge about the workspace and the target objects.

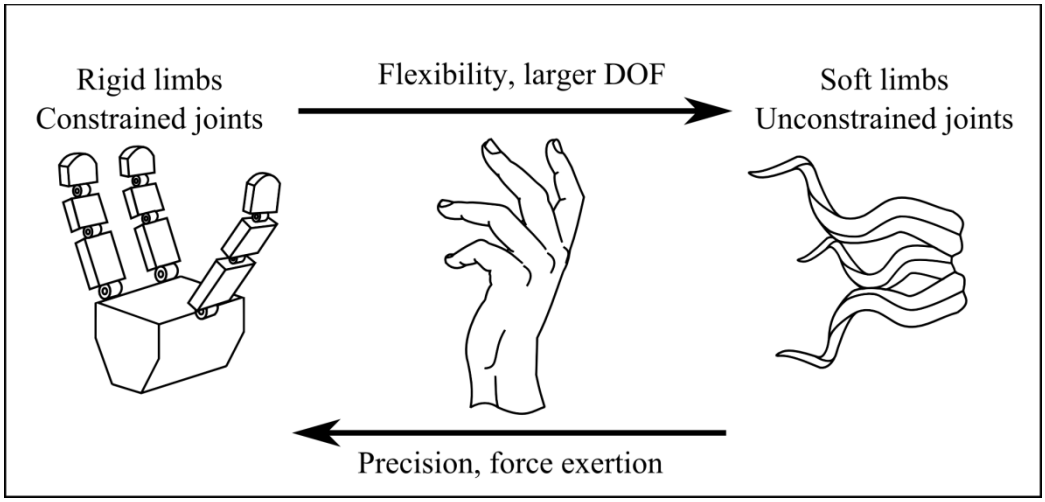

Figure 1. The choice of anthropomorphic robot hand lying in between two extreme ends of robotic hand designs. To one end, rigid limbs that attached to each other with hinge type joints manifest precise control and the ability to exert large amounts of force but inflexible structure and fragile interaction. To the other end, completely soft limbs and virtually infinite degrees of freedom allow enhanced conformity and softness during interaction but reduced actuation control capacity.

Robotic hands that belong to the second approach, such as Hirose [14], Pisa/IIT [15], FRH4 [16], SDM [17], iYH [18], Cianchetti [19] and RBO 2 [20] use soft deformable materials instead of fixed DOF mechanisms at their joint locations. These robots are generally underactuated due to having larger DOF than their actuators; however they show important progress in demonstrating passive compliance during interaction by relying on the mechanical adaptation capacity of their joint and

finger designs. Unlike in the joint designs in the first approach, less constrained joints that generate larger DOF allow multi-directional compliance and let these designs to exploit environmental niche and interaction physics to adaptively grab and manipulate objects [21,22]. Additionally, such hand designs reduce the computational load on feedback controllers, and make use of soft interaction physics with the environment [23]. However, these hands mainly face two problems: (1) the softness of their joints or limbs hinder their force exertion capacities, and (2) having a larger DOF than the limited number of actuators increase the gap between actuation and posture space.

When these two groups of approaches are compared, it can be seen that passive compliance and how it is maintained, mainly describe the behaviour of the hands. At one end, the direction of the compliance is defined by and constrained into fixed axis of motion with special joint designs such as hinges and gimbals. And at the other end, these constraints are effectively loosened by joints with soft and deformable materials that allow multi-directional compliance. From the perspective of anthropomorphic hand and robotics research, finding a solution in between these two end points is a motivating objective. Such an approach will be addressing the challenges in how to regulate the directions of joint compliance by structural design and use of different materials, yet still maintaining a sufficient amount of force exertion and establishing a closer actuator-finger posture relation. Hands that are designed this way will be bringing the advantages of both ends together, making them more adaptive, less dependent on active control, stronger in grasping forces and less fragile during interactions with environment.

In those terms, human hand joint design presents a valuable example; however researchers have not yet integrated the actual source materials, i.e. anthropomorphic elements of the joints. Bones, elastic ligaments, synovial fluid and muscles/tendons together contribute to the passive compliance of the human hand joints, but researchers preferred to mimic the behaviour of a part of them so far. To best of our knowledge, the joint design closest to a complete integration is the variation of the ACT Hand's joint which replaces the hinge and gimbal type mechanisms with anatomically correct bones and ligaments [24]. Although these artificial joints have close fit with their human counterpart's features, the elastic capacity of the joints during object or finger interaction are not demonstrated.

In this paper we are presenting our compliant anthropomorphic joint design to achieve multi-directional compliance by applying a bio-inspired solution in between two ends of hand joint design approaches. Differing from other robotic hands, we use anthropomorphic design elements like bones, multiple elastic ligaments and tendons in order to build our joints and regulate their DOF and passive compliance. We build a robotic hand with an index finger and a thumb which are actuated with fourteen antagonistic tendons. Our experiments aim to enhance the range of motion of our fingers with interactions between the index finger and the thumb, and extend the gripping size with a resizable object larger than the natural grip size. We show that our anthropomorphic design can tackle various shortcomings of other groups of robotic hands. The bone cavity geometry, tendon routings and the multi-layer elastic ligament encapsulation can provide multi-directional passive compliance during physical interactions and enable the extension of finger motion ranges. Also the rigid bone structure along with high tensile strength tendons allow the transfer of actuator torque to finger tips for more effective force exertion. Lastly, overall design contributes to an establishment of actuator to finger posture relation which is an important premise for underactuated robot control.

In this perspective, our platform aims to have a better understanding of human hand by experimenting on joints' role in the finger functions, the relationship between multiple tendons and finger positions, and the role of passive compliance during object interactions. Additionally, it suggests a template for future directions to explore learning motor control of underactuated fingers, investigate distributed tactile sensing and impact recovery. In conclusion, we believe that our research can contribute to the development of improved prosthetics and broadening of human-robot interaction with more recognizable robot hands that can perform better and safer around humans.

The structure of this paper is as follows. In chapter 2 we aim to provide information about our methods for defining the anthropomorphic model, the materials we use, how to build the fingers, the actuation mechanisms and the visual feedback platform we use for experiments. We show the natural range of motion of the fingers and how this range is extended with active finger interactions via experiments in chapter 3. We discuss the features of our fingers, and how they can be improved in future works and conclude our work in chapter 4.

2. Methods

2.1. Anthropomorphic Model

Human hand is a complicated organ consisting of 27 bones, about 40 muscles and more than 25 DOF [1,5]. In this paper, we only focus on the details of the thumb and the index finger, which have important roles in the overall hand functions [25-27]. Both fingers have a metacarpal, proximal and distal phalange, where index finger has an additional middle phalange in between metacarpal and the proximal. The joints between these phalanges are called Distal Interphalangeal (DIP), Proximal Interphalangeal (PIP) and Metacarpo-phalangeal (MCP) for the index finger and Interphalangeal (IP), Metacarpo-phalangeal (MP) and Carpometacarpal (CMC) for the thumb. We are using the abbreviation "MP" for the thumb metacarpo-phalangeal joint to distinguish it from the index joint with the same name. The DIP, PIP of the index and IP and MP joints of the thumb has 1DOF, where MCP of the index has 2 and CMC of the thumb has 3 DOF. There are a number of pulley locations, namely A1-A5 in index and A1-A2 on thumb, for the routing of tendons over the phalanges. The complex ligament shell around the joint gaps holds the synovial fluid, which generate low friction on the bone surface, while providing structural elasticity.

By looking at the anatomy of the right hand, we define our anthropomorphic fingers to a level of bio-mimicry. Figure 2 (a) shows the dorsal view of the simplified tendon arrangement we define in our robotic hand. There are three sets of antagonistic tendon pairs for the index finger and four for the thumb. These tendons go through pulleys, whose locations are inspired from their anatomic counterparts to provide basic finger motions such as flexion/extension and abduction/adduction. While all the pulleys and tendons remain on the index finger, the adductor tendon of the thumb's metacarpal goes through the metacarpal of the middle finger in order to mimic the adductor muscles in the palm. The tendons also help the translation of actuator torque to joints and finger tips.

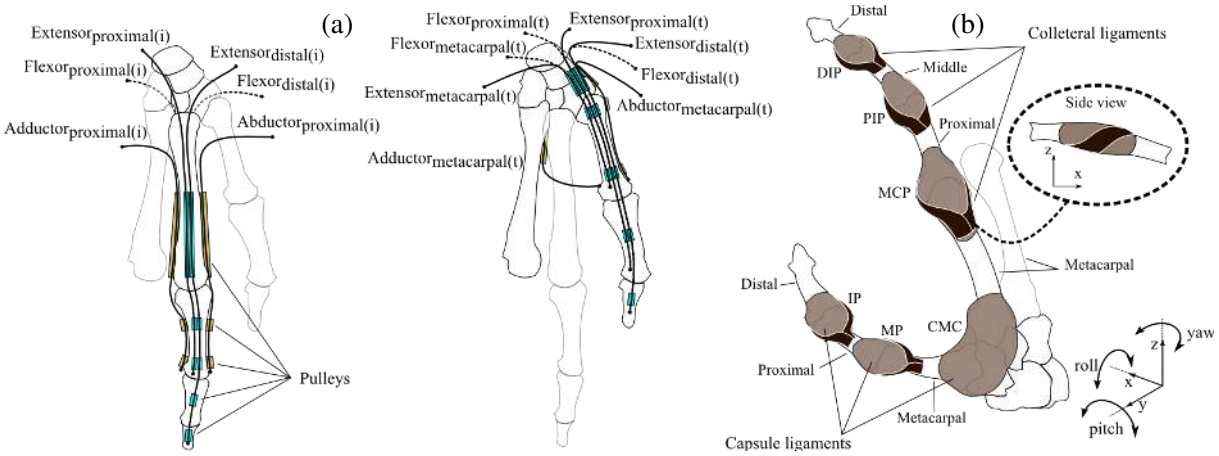

Figure 2. The model of suggested anthropomorphic robotic hand design. (a) Palmar view of tendon and pulley placement. Tendons are named after their function, the phalanx they are attached to and the initial of the finger they belong as in *"function$_{anchor}$(finger initial)"*. Flexor and extensor tendons of the same phalanx are shown overlapped, flexors with solid and extensors with dashed lines, as they follow exact routes on opposite sides of the finger. (b) Elastic ligaments are used to cover the finger joints where the capsule ligament is the inner shell that covers the whole joint and collateral ligament is attached on the sides to give additional stability. A side

view of an index finger joint shows how ligaments are connected in the zooming clip. Principal axes of the reference frame are shown for the definition of angular motions.

The passive compliance of the human fingers is mainly provided with the elastic constraints around the joints defined by the ligaments; therefore in our model we use anatomically correct finger bones which are covered with two types of elastic ligaments as shown in figure 2(b). The first type of ligament, capsule ligament, is a layer of protective and stabilizing tissue around the joints. This elastic layer keeps the joints in place and allows bone tips to slide over each other during the motion. The second ligament, collateral ligament, is a stronger tissue which surrounds the sides of the joints to guide the motion in addition to the bone tips. In our model, collateral ligaments are shaped and placed similar to the biological ligaments, so that they can constraint the motion to one or two DOF depending on the joint. Unlike the actual anatomy, we do not used collateral ligaments on the CMC joint, whose DOF and elasticity is only guided by the capsule ligament.

2.2. Materials and Fabrication

Similar to human hand, our robotic hand is made of different types of materials that are integrated in a confined space. When the overall mechanism is concerned, our hand can be classified as soft because the finger functions are mainly due to the deformation of the relevant materials around the joints, in contrast to mechanisms like rolling pins or hinges. When a force is applied, the tendons transfer this force over the comparatively rigid bones, to their attachment points. While this structural transfer generates a torque, this torque acts on the deformable soft material around the joints and results as one or a combination of finger functions like flexion, extension, abduction or adduction.

In order to reach anatomic accuracy, we use the bones of the right hand from skeletons provided by 3B Scientific GmbH, Germany. This hand skeleton model preserves the anatomical details of the bone tips which play important role during the motion of the finger bones under applied torque. The bones are made of PVC plastic with an approximate 67 MPa tensile strength; therefore they behave as rigid bodies within the force range generated by our system. In our paper we only use the bones of the index finger, the thumb, the metacarpal phalange of the middle finger and trapezoidal bones of the wrist for structural completeness; however only the index finger and the thumb are actuated. The physical parameters of the actuated bones are given in table 1.

Table 1. The physical parameters of the index finger and thumb.

Finger	Phalange Name	Length (mm)
Index	Distal	16
	Middle	24
	Proximal	38
	Metacarpal	70
Thumb	Distal	24
	Proximal	31
	Metacarpal	48

Human finger joint structure is a multi-layered mechanism composed of several collagen and elastic fibre based tissues covering the bones and the joint cavity. Anatomical research shows the main contributor to joint stability and motion are tendon and muscle forces; however the ligament structures are the first level tissues that play important role in passive stability and elasticity [28]. In our paper, we focus on the two ligament tissue layers: the joint capsule and collateral ligaments. As the first layer of tissue that spherically covers the joint cavity, joint capsule binds the bones together, encapsulates the joint cavity to store the synovial fluid and provides passive elasticity to the joints [28]. Compared to the joint capsule, collateral ligaments have a denser collagen structure that makes them more stable

while they connect the bones to each other as sheets of ligaments of several layers [29]. Both of these elements are crucial in the general adaptivity and the stability of the human fingers.

Inspiring from the anatomical structure of the human joint we are using two different types of elastic materials for the ligaments which are the main sources of deformation in the robotic hand. The first one is the capsule ligament which completely covers the joint space in between the bones. We are using black nitrile rubber (NBR sheet, White Cross Rubber Products, UK), which is widely used for manufacturing medical examination gloves, that has approximately 5 MPa of tensile strength. This material is strong enough to keep the bones attached to each other and preserve the gap between the bone tips at minimum. It can also elongate under applied torque to generate the bending motion of joints. The second one is the collateral ligament which winds around the bone gap for torsional stability on the phalanges. We use black butyl rubber, (Butyl IIR sheet, White Cross Rubber Products, UK) that has an approximate 7 MPa tensile strength which makes it more resistive to strain compared to the capsule ligament, but elastic enough for joint compliance. These two types of materials are chosen to mimic the multi material ligament composition and their co-related elasticity influence in the real human hand ligaments, but not to replicate their actual quantitative elasticity properties.

The tendons which carry the output force to the bones are made of 0.55mm diameter Dyneema® PE braided fishing lines with 3.1 GPa tensile strength. Considering the force output of the actuation system, these tendons do not elongate under stress, therefore making the experiments repeatable. The pulleys which the tendons go through are made of Polytetrafluoroethylene (PFTE tubes, Farnell, UK) with Teflon coating which generates a low friction inner surface. In order to assemble and glue the required materials to each other, we use a thermoplastic elastomer variant hot melt adhesive (HMA, Pattex, Henkel, UK). When heated up, this material turns into viscous liquid form and fills the gap between two complex surfaces to make a bond when cooled down. Previous studies in our laboratory shows that this material can create strong bonds between multiple materials, and can resist to tensile and shear stress even on small surfaces [30]. Under the guidance of these studies, we choose to use this material to create continuous and strong bonding surfaces between the PVC based bones and rubber based ligaments in our joints.

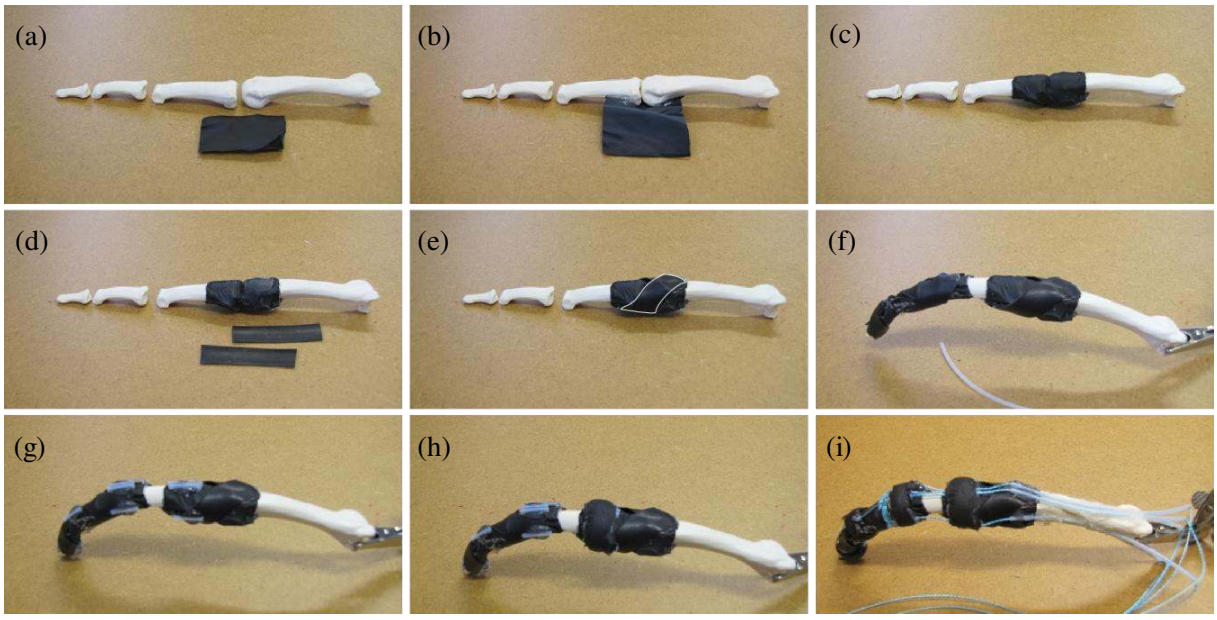

Figure 3. Fabrication stages of the index finger. Capsule ligament is covering the joint cavity by attaching to end parts of bones with hot melt adhesives (a-c). Collateral ligaments whose geometry is highlighted in (e) are placed on the side for torsional stability of joints (d-e). Remaining joints are covered with ligaments with the same method (f). Low friction short tube pieces are placed on anatomically inspired pulley positions (g). Pulleys are

fixed with additional hot melt adhesives and nitrile rubber to withstand torques (h). Tendon cables are routed through pulleys and longer tubes on non-moving bones (i).

Due to the complexity of the anatomically correct pieces and continuum surfaces we assemble our fingers by hand as shown in figure 3. First we cut 30x30 mm sheets of nitrile rubber with 0.1 mm thickness to surround the bone cavity. These pieces are glued to the tips of the bones by leaving a small gap (~0.2 mm) between to allow the bones to slide over each other while moving under torque. We glue the collateral ligaments on top by cutting 10x30 mm sheets with 0.7mm thickness. Inspired from the natural example, these ligaments make a twist around the joint by attaching the top of the base bone to the bottom of the follower bone. We repeat the ligament attachment process for every joint, excluding the CMC from collateral ligaments.

When the ligaments are complete, we start gluing the pulleys by cutting small pieces from the low friction PFTE tube on the fingers. Each pulley is a tube with 1mm diameter and 10 mm length which is placed similar to the locations of A1 to A5 pulleys on the index finger and A1-A2 pulleys on the thumb. We mimic the adductor muscle of the thumb by placing a pulley on the metacarpal of the middle finger. Longer tubes are placed on the metacarpal phalange of the index and middle finger and the glued wrist bones to route the tendons from the joints to the actuation mechanism. In order to increase the strength of the pulleys against the torque generated during bending motions, we use additional glue and nitrile rubber to make fixation rings around the pulleys. We place the 0.55 mm diameter tendons at the last stage of the assembly by pulling them through the tubes and pulleys. We fix the anchor point of the tendons on the bones by knotting and gluing, while the other end is kept free to be attached to the actuation mechanism.

The overall assembly takes approximately 3 hours with the index finger, thumb, the metacarpal of the middle finger and the wrist bones. The resulting robot hand, which weighs 70 grams, has 14 tendons and two actuated fingers, can be seen in figure 4(b).

2.3. Actuation Mechanism

The actuation mechanism of our robot hand consists of 14 tendon driving modules which can be controlled independently from each other. Each module has a microcontroller, a motor driver, a 100:1 gear ratio Pololu® 6V DC motor with 0.22Nm stalling torque output, and a motor encoder for position feedback inside a 30x40x50 mm box. There is a pulley with a circumference of 22mm attached to the motor shaft, which is connected to the free end of a tendon. These modules are connected to each other over a master communication unit with an I^2C bus. Each module runs a PD controller loop whose target position can be set by computer and transferred to the master communication unit with a USB connection. Complete platform is shown in figure 4.

Due to the position encoder, circumference of the motor pulley and tendons with high tensile strength, we can control the rotation of the motors up to 0.3° and stroke of the tendons up to 0.02 mm precision. The precise control of the motors also allows us to detect stalls without any additional sensor unit. When a single tendon driver module is commanded to pull a tendon to a certain target value, the position and the rotational velocity of the motor shaft can be monitored to check if the motor is stalling. By using the PD controller in each module, we can detect a stall when the error between the current and the target tendon stroke is larger than a tolerance amount, 0.5 mm in our case, and the motor velocity is zero.

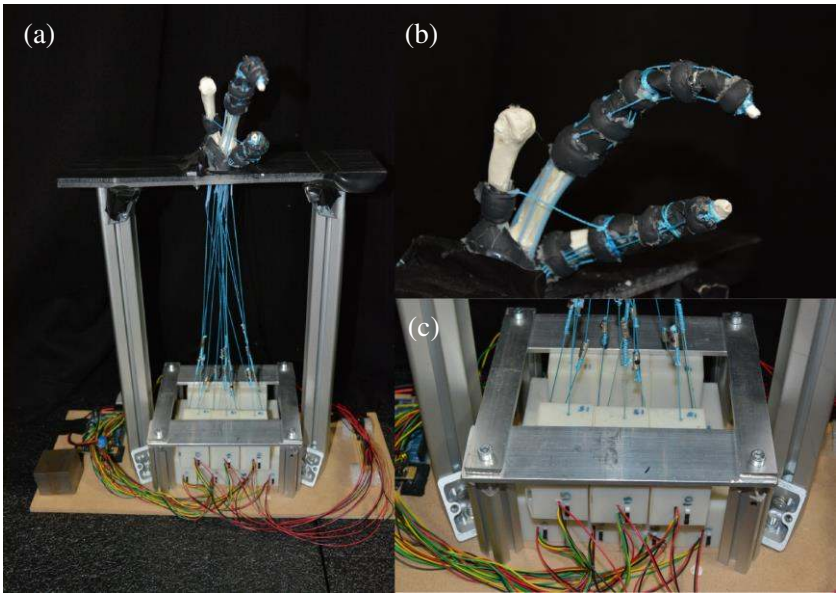

Figure 4. Complete platform which hosts the assembled fingers and the actuation mechanism (a). The index finger, thumb and the middle finger metacarpal are connected to wrist bones and fixed on top of the platform (b). There is one actuation module for every tendon which is controlled with a micro controller (c).

2.4. Motion Capturing

The complexity of the hand structure and the soft joints in particular make it impossible for our platform to derive inverse kinematics and relate tendon to finger positions. As we do not implement an on board soft sensor in this research, we are gathering the 3D position information of the fingers from a motion capturing setup.

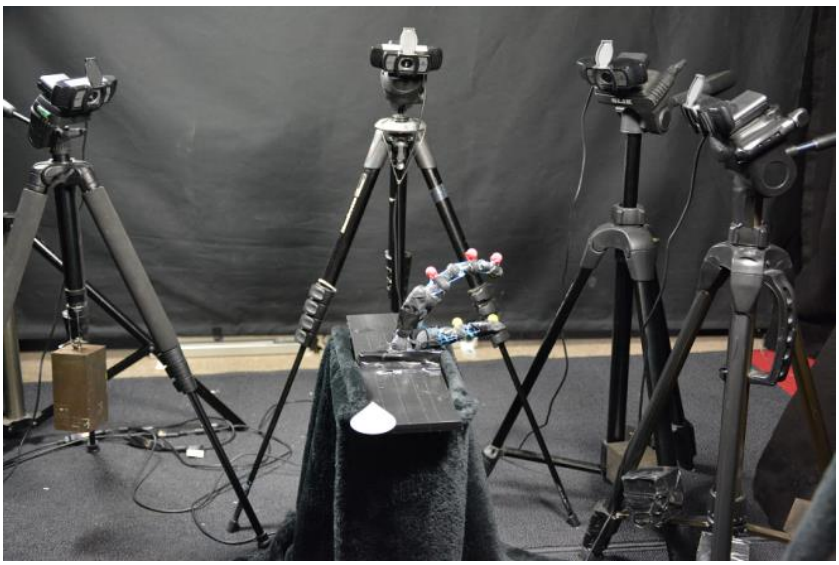

Figure 5. Motion capture setup which tracks colour markers on the fingers with four different cameras. Each phalange has a colour marker attached to it, making six markers in total. There is a white marker on the surface of the platform to set the reference frame.

As shown in figure 5, our motion capture arena has four high definition web cameras which focus on the hand platform in the centre. These cameras are placed so that at least two of them see all of the markers at a single time instance. We place red markers on each actuated phalange of the index finger and yellow for each actuated phalange of the thumb. There is also a white marker on the surface of the

platform to fix the reference frame. The arena is covered in black to generate a high contrast scene for the images that we capture from the cameras.

We use MATLAB ® and its computer vision system toolbox [31] to perform the 3D reconstruction of our fingers from camera images. First, we use the camera calibration application from the vision system toolbox to calibrate the cameras and produce the camera matrices that give information about the intrinsic, extrinsic and the lens distortion parameters. This is done by placing a checkerboard pattern picture, whose size, length and amount of squares are known and registered to the toolbox, in various poses within the range of all four cameras. Each pose of the checkerboard is captured as images and the corner points on the checkerboard pattern are detected in each camera image. As the real size of the checkerboard is known, the detected corner points and their geometry in the images allow the calculation of the 3D space pose of the checkerboard and the relative position of all the cameras to each other. In order to follow the hand postures, we use a simple RGB colour filter algorithm to detect the markers on the captured images. These detected marker positions and camera matrices are related to each to reconstruct a 3D scene from captured 2D images using a customised version of Direct Linear Transformation (DLT) algorithm [32]. Only the images which detect seven colour markers are considered as the source for triangulation in our algorithm.

3. Results

3.1. Tendon Stroke Limits

Before every experiment, tendon calibration is necessary to ensure a repeatable and reliable platform. As we control the position of the fingers with tendon strokes, it is substantial to make sure that tendons are always in their correct position. In order to do so, we release all the tendons to begin the calibration process. Following that, we pull every antagonistic tendon pair with a stroke step of 0.1mm simultaneously until a motion on the relevant finger is detected by the motion capture system. The last value of the tendon stroke which did not generate a motion is registered as the resting position of that particular tendon and stored as a reference value. This ensures a minimum necessary pre-tension on the tendons and consequently calibrates the platform.

After calibration, we start our experiments with detecting the stroke limit of each tendon until the load from its attached joint causes a stall at the actuating motor. In this experiment, each tendon is pulled with a stroke step of 0.2 mm until the motor stall is detected as explained in Section 2.3. While a tendon is being pulled, all other tendons are kept at resting position to incorporate the resisting effect of antagonistic tendon pairs and elastic ligaments. Therefore, given the current setup, tendon stroke limits also represent how much tendons can be pulled with our actuators. Figure 6 shows the maximum strokes for each tendon until they reach their load limit of the motors.

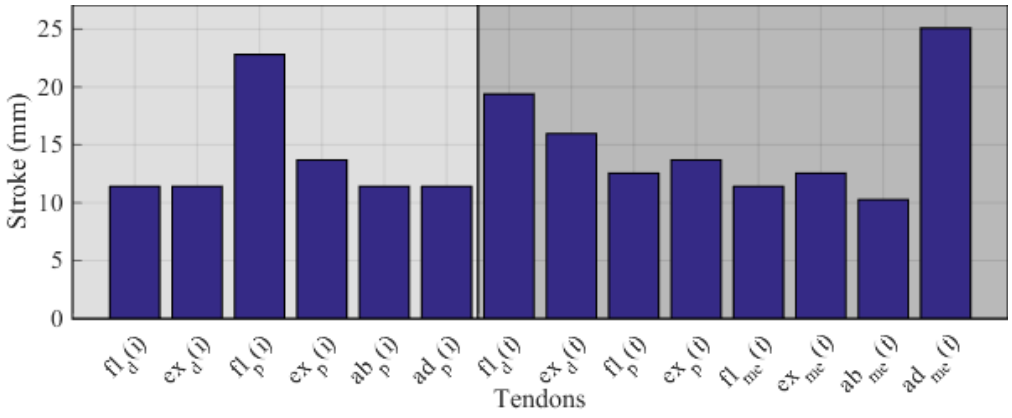

Figure 6. Maximum stroke of tendons at the load limits of their actuators. The six tendons in the light shaded region belong to index finger, and the other eight tendons in the darker region belong to the thumb. (We use

abbreviated versions of tendon naming; flexor: fl, extensor: ex, abductor: ab, adductor: ad, distal: d, proximal: p, metacarpal: me)

We see that the maximum strokes, or load limits, generally have similar values for antagonistic tendon pairs of the same phalange as flexor-extensors and abductor-adductors. However there are several exceptions like the flexor-extensor of the index proximal and abductor-adductor of the thumb metacarpal. The main reason for the difference in the formal case as the flexor $fl_p(i)$ can be pulled more than the extensor $ex_p(i)$ is the geometry of the bone tips and the mechanical constraint it enforces on the joint motion. We can explain the difference between the adductor and abductor of the thumb metacarpal, i.e. $ab_{me}(t)$ and $ad_{me}(t)$, by the effect of a larger space for motion given by the tendon routing over the middle finger metacarpal.

3.2. Range of Motion

First of all, we find the joint motion limits by manually exciting the phalanges. During this experiment, tendons are not active to show the physical limits of the joint mechanisms which are defined by the elasticity of the ligaments and the bone anatomy. Those limits, as seen in table 2, show similarity to the actual limits of human hand reported in literature [5,33,34].

Table 2. Finger joint motion limits

Finger	Joint	Minimum	Maximum	Human Hand
Index	DIP	60° extension	80° flexion	50.4°±6.6° (flexion/extension)
	PIP	25° extension	110° flexion	89.5°±11.7° (flexion/extension)
	MCP	30° extension	70° flexion	85.3°±18.4° (flexion/extension)
		35° abduction	35° adduction	50.4°±6.6° (abduction/adduction)
Thumb	IP	60° extension	90° flexion	80° (flexion/extension)
	MP	40° extension	80° flexion	70° (flexion/extension)
	CMC	35° extension	40° flexion	45° (flexion/extension)
		35° abduction	40° adduction	40° (abduction/adduction)

Range of motion of human fingers are adopted from [33] for index finger and [34] for thumb

After acquiring the tendon limits, we explore the active range of motion of the joints by doing an exhaustive search on the tendon stroke combinations. For this, we define $S_j(i)$ for index finger and $S_j(t)$ for thumb, which show the stroke state of a tendon j; in either of pulled to limit or relaxed. "Pulled to the limit state" means that the tendons are pulled to the limit stroke values which are shown in figure 6. "Relaxed state" means that the tendon is released to the negative motor direction with half the magnitude of its load limit. This ensures that the search also looks for the combination where antagonistic tendon pairs can function effectively without generating resistive pulls in counter acting motions. Considering the two phases, we search 2^6 combinations for the index finger and 2^8 for the thumb. In order to avoid the effect of physical interactions between two fingers, we run the tests for each finger separately.

By using customised DLT algorithm repeatedly, we detect the location of markers on the finger phalanges and generate a 3D reconstruction of the hand for the pose it takes as a result of each action within the tendon combination set. We take a single, constant base point of the hand as the middle point between the trapezoid and trapezium bones in the wrist, which is calculated with respect to the reference frame, fixed on the white marker. For every 3D point space resulting from a tendon action, we calculate the angle between the each phalange and this base point on three basic axes, i.e. yaw, pitch and roll for all of the experiments. Then we collect these angles to represent the range of motion of the fingers given the limits of the tendons, which can be seen in figure 7.

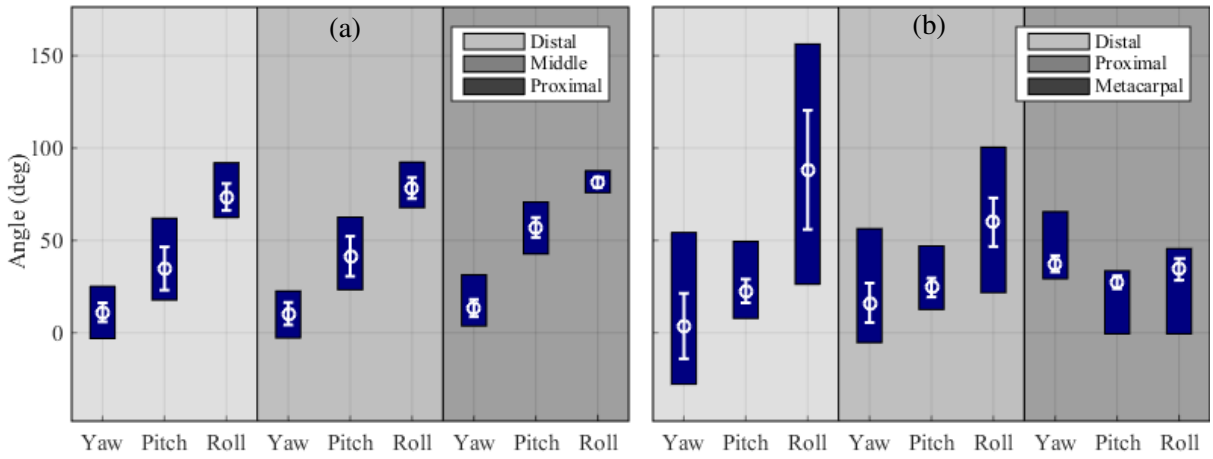

Figure 7. Each shaded column represents a finger phalange with its range of motion in yaw, pitch and roll angles. Index finger phalanges are shown in (a) and thumb phalanges are shown in (b). Coloured bars on the figure show the distribution of angles, where white lines show the standard deviation and white circles show the mean of this distribution.

The range of motion shown in figure 7 are the results of all the tendon actions acting on the fingers separately, meaning that there are no interactions between the fingers or with the environment. The choice of representing the range of motion in three principal axes with respect to a single base point has several advantages from the perspective of our paper. First, it can show the possible overlapping workspace of the index finger and the thumb, which is an important indication to possible interactions between fingers that can influence motion range. Second, one dimensional lines in these three principal axes can more clearly represent the scalar values of range of motion of bodies in 3D space and how they will be extended with finger interactions, which will be shown in the following sections. Third, it demonstrates the results of multi-directional compliance of the joints, which can be seen as motions in 3D space. And lastly, as our system is underactuated and the influence of tendons on phalange motions are correlated, this representation is useful to establish the tendon action-phalange angle relation which will be discussed in the next section. Table 3 shows the quantification of the range of motion of each phalange at the end of the experiments.

Table 3. Range of motion of the thumb and the index finger without external interaction

Finger	Phalange	Yaw (°)	Pitch (°)	Roll (°)
Index	Distal	28.2	44.1	29.5
	Middle	25.4	39.3	24.7
	Proximal	27.7	28.0	11.9
Thumb	Distal	82.1	41.6	130.0
	Proximal	61.6	34.4	78.6
	Metacarpal	36.3	34.1	46.1

The gist of table 3 shows that each phalange exhibits motion in all of three axes. In addition to the multi-directional joint compliance, this is a direct result of exhaustive search on tendon action combinations where tendons working on perpendicular axes; e.g. flexor and abductor, can be pulled together at the same time. However, these results can still be compared to table 2, when the principal motion axes of tendon actions are taken into consideration. Although motions in three axes are co-related, the main influence of flexion/extension actions of the index finger can still be seen in the pitch axis, and the abduction/adduction can be seen in the roll and yaw axes of the index phalanges in table 3. Similarly, the flexion/extension of the thumb can be seen in the roll and yaw, and abduction/adduction can be seen in pitch axis of thumb phalanges.

3.3. Tendon Action to Phalange Angle Relation

Due to the soft and deformable nature of the joints which yield a greater number of DOF, i.e. this can be regarded as virtually infinite, compared to the controllable DOF with 14 tendons, deriving an analytical formula between the tendon actions and the resulting finger positions is a challenging task. That is why, in this paper we deduce this relation by collecting the experimental data.

We define the sets $A_j^k(i)$ for index finger and $A_j^k(t)$ for the thumb, where each set contains the yaw, pitch and roll of each phalange for the state of the tendon j in the k^{th} combination of tendon actions. To find the effect of tendon j in the index finger as $E_j(i)$, we traverse the whole combination set and find the difference between the mean of the angle sets when the tendon is pulled, i.e. $T_j^+(i)$, and when tendon is released, i.e. $T_j^-(i)$ as follows:

$$T_j^+(i) = \sum_{k=1}^{2^6} mean\left(A_j^k(i)\right), for\ S_j(i) = pull \qquad (1)$$

$$T_j^-(i) = \sum_{k=1}^{2^6} mean\left(A_j^k(i)\right), for\ S_j(i) = release \qquad (2)$$

$$E_j(i) = T_j^+(i) - T_j^-(i) \qquad (3)$$

The resulting figure 8 (a) shows important characteristics of the index finger actuation. First, we see that flexors have a negative, and extensors have a positive effect on the pitch angle of all the phalanges. We see the same opposing effect between the antagonistic pairs of abductor and adductor tendons on the yaw and roll angles of the phalanges. However, this figure also shows the coupled effects due to the under actuation of the finger. Although smaller in magnitude, we see that flexor and extensor tendons can also influence the roll and yaw angle of the finger, giving us the hint of the possible actuation exploitations of underactuated anthropomorphic joints.

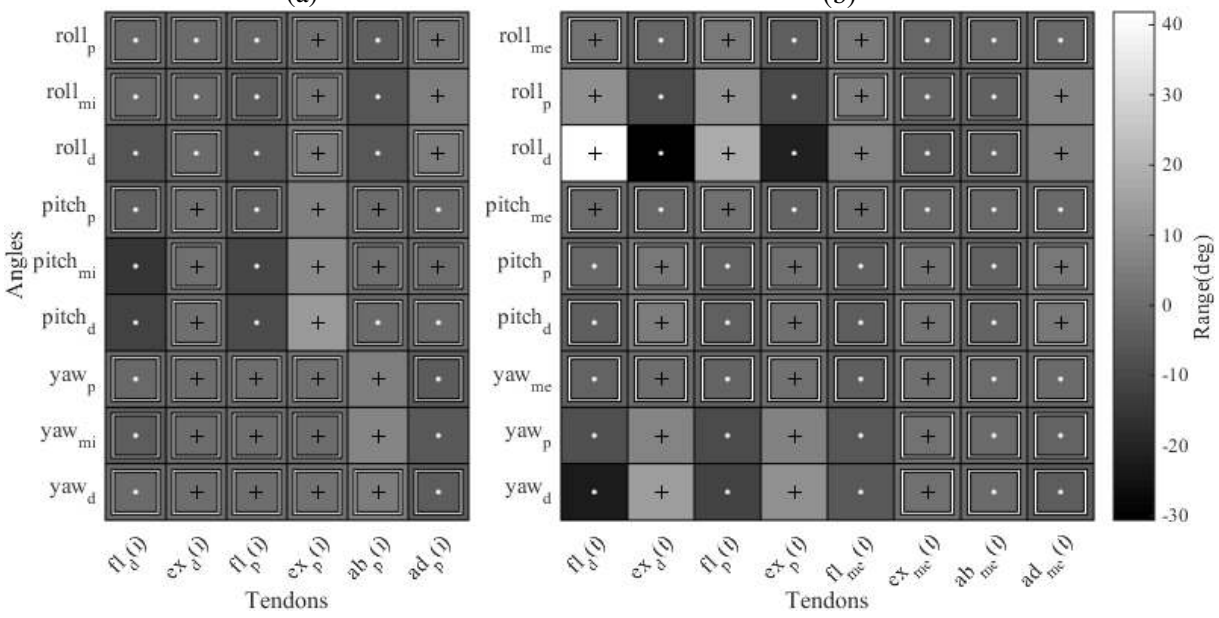

Figure 8. Impact of each tendon on the range of phalange angles of index finger (a) and the thumb (b). The colour of the shaded boxes shows the direction and the magnitude of each tendon's action on phalange angles in yaw, pitch and roll axes. While the range changes from -30° to 40°, the light colours towards white represent the increasing positive effect and dark colours towards black represent the increasing negative effect. In order to aid the visualisation, positive effect boxes are marked with black plus and negative boxes are marked with white dot markers. Additionally, boxes that are within range of -5° to 5° are marked with white border inline to show the zero or small angular effects from the tendons.

We perform the same experiment on the thumb to find the effects of j^{th} tendon in $E_j(t)$, with $T_j^+(t)$ and $T_j^-(t)$ are defined as:

$$T_j^+(t) = \sum_{k=1}^{2^8} mean\left(A_j^k(t)\right), for\ S_j(t) = pull \quad (4)$$

$$T_j^-(t) = \sum_{k=1}^{2^8} mean\left(A_j^k(t)\right), for\ S_j(t) = release \quad (5)$$

$$E_j(t) = T_j^+(t) - T_j^-(t) \quad (6)$$

and whose results are shown in figure 8 (b). It can be seen that the flexors are increasing the roll range while decreasing the yaw and pitch. The complete opposite of this holds true for the extensor tendons. Due to the larger DOF in the CMC joint, the effects of tendons on the thumb are greater compared to the index finger. As there is a tendon pair actuating every joint of the thumb, the clear distinction of their effect is more visible in this figure, compared to the coupled effects of the underactuated index finger.

3.4. Using finger interactions to extend range of motion

In order to exploit the elasticity of our anthropomorphic joints, we use finger interactions to push them in different directions to show the multi directional passive compliance and its implication on the extension of range of motion. As the comparative range of motion experiments hint in figure 7b, the thumb has a larger range within the same workspace with the index finger; therefore it can be used to push the index finger out of its normal range.

For this, we experiment on three behaviours: abduction, adduction and flexion of the thumb. All experiments have two phases: the setup phase and the action phase. In the setup phase, we actuate the fingers to their respective initial places and in the action phase, the thumb is actuated to perform one of three behaviours. We record the tendon activity in both phases and the normal force acting on the index finger tip in the action phase. We use a spring scale attached in series to the tip of the thumb and align it on the axis of pushing motion to track the force exerted on the index finger by the thumb. These experiments can also be seen in detail from the video attachment.

3.4.1. Abduction Experiment. In the setup phase of this experiment, thumb is adducted towards the middle finger, staying behind the curled index finger as shown in the leftmost picture of figure 9 (a). When the setup is complete, all of the extensor tendons of the thumb are pulled to their limit within 4 seconds while the index finger flexors are pulled constantly at their curling positions. The final pose of the fingers can be seen at the rightmost picture of figure 9 (a). During this action phase, the normal force, F_{abd}, acting on the index finger tip goes up to 2N at the last step which can be seen alongside with the tendon excursions in figure 9 (c).

When we look at the range of motion during the abduction experiments in figure 9 (b), we see that there is an increase of 47% in the roll range of the distal phalange on the lower end. There is also a small increase, namely 6.2% and 4.7%, in the pitch and roll range of the proximal phalange.

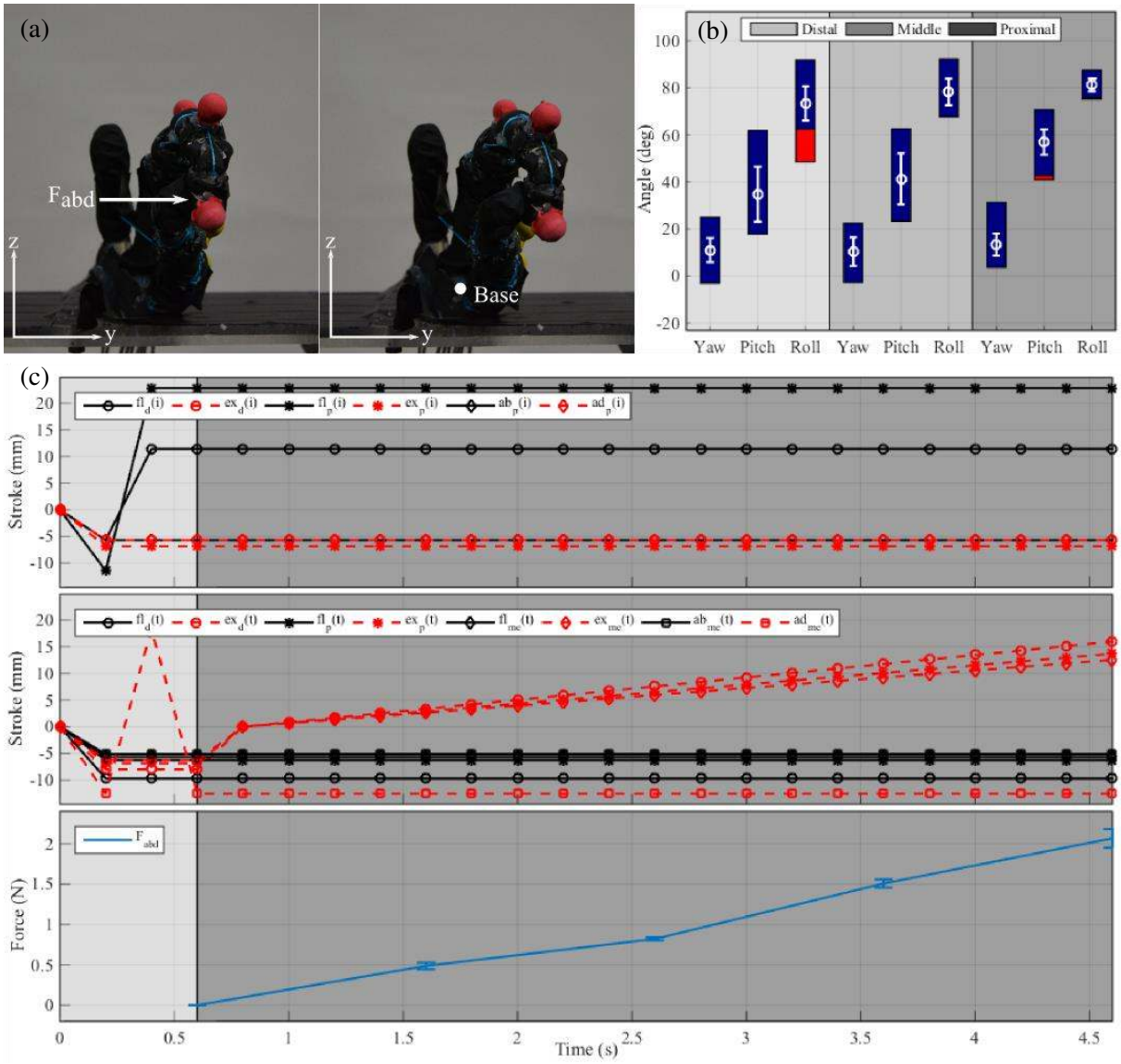

Figure 9. Abduction experiment. The initial (left) and the final (right) poses of fingers are shown with the direction of the pushing F_{abd} force (a). The extension of index finger's range of motion is shown with red bars added to the normal range in figure 7 (b). Top and middle figures are showing the tendon excursions of both fingers in setup (light shade) and action (dark shade) phases. Bottom figure shows the normal force acting on the index finger's tip during action phase (c).

3.4.2. Adduction Experiment. In the adduction experiment, the thumb is actuated towards the outer side of the index finger which can be seen in figure 10 (a). In the action phase, the distal and proximal flexors along with the metacarpal abductor of the thumb are pulled slowly to their limit to push the index finger towards the middle finger. In this motion the normal force F_{add} reaches up to 4N towards the end of the action, whose relation to tendon excursions can be seen in figure 10 (c).

Compared to the previous experiment, the increase of range of motion is larger with the adduction. We see an increase of 52.2%, 29.1% and 197.5% range in the yaw, pitch and roll of the distal phalange. The roll increase is in the higher end of the range due to the direction of the acting force. This motion also has a small increase of 7.7% on the range of middle phalange's roll which can be seen in figure 10 (b).

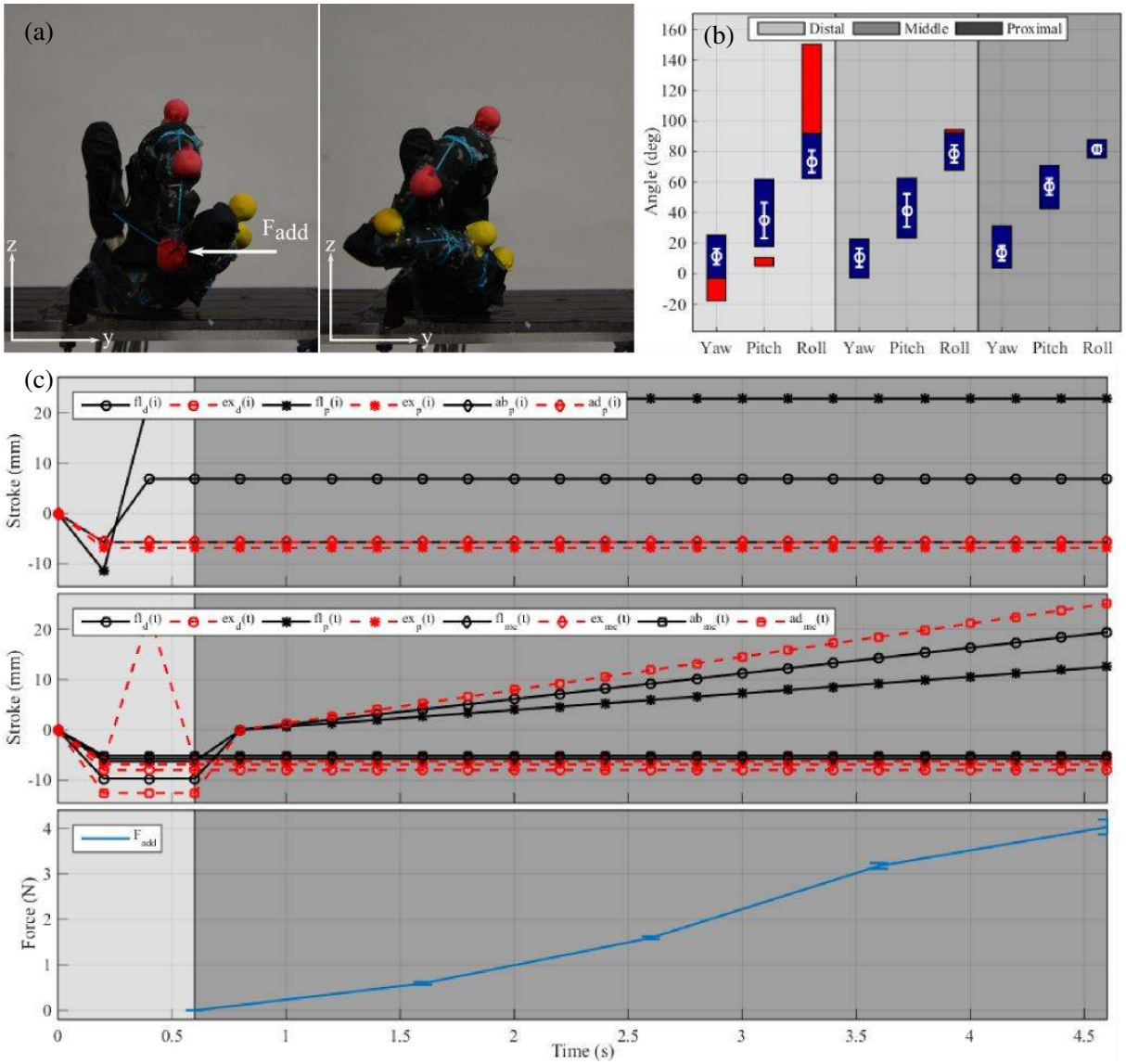

Figure 10. Adduction experiment. The initial (left) and the final (right) poses of fingers are shown with the direction of the pushing F_{add} force (a). The extension of index finger's range of motion is shown with red bars added to the normal range in figure 7 (b). Top and middle figures are showing the tendon excursions of both fingers in setup (light shade) and action (dark shade) phases. Bottom figure shows the normal force acting on the index finger's tip during action phase (c).

3.4.3. Flexion Experiment. In the last experiment, we place the thumb on top of the index finger to push it towards the base whose initial and final poses can be seen in figure 11 (a). In the setup phase of this experiment, after the thumb is actuated to its final position, the tendons of the index finger are released to show the effect of the interaction force F_{flx} only. In the action phase, the flexors of the distal and proximal along with the adductor of metacarpal are pulled while the metacarpal extensor is pulled to a constant value to keep the shape of the thumb. These tendon actions generate a normal force that goes up to 1.8N on the index finger which can be seen in figure 11 (c).

The flexion experiment has a similar effect to adduction experiment on the range of motions which can be seen in figure 11 (b). We see that the distal phalange experiences an increase of 41.4%, 13.8% and 169.2% range in its yaw, pitch and roll. There is a small increase of 1.1% on the yaw and 15.5% in the roll of the middle phalange.

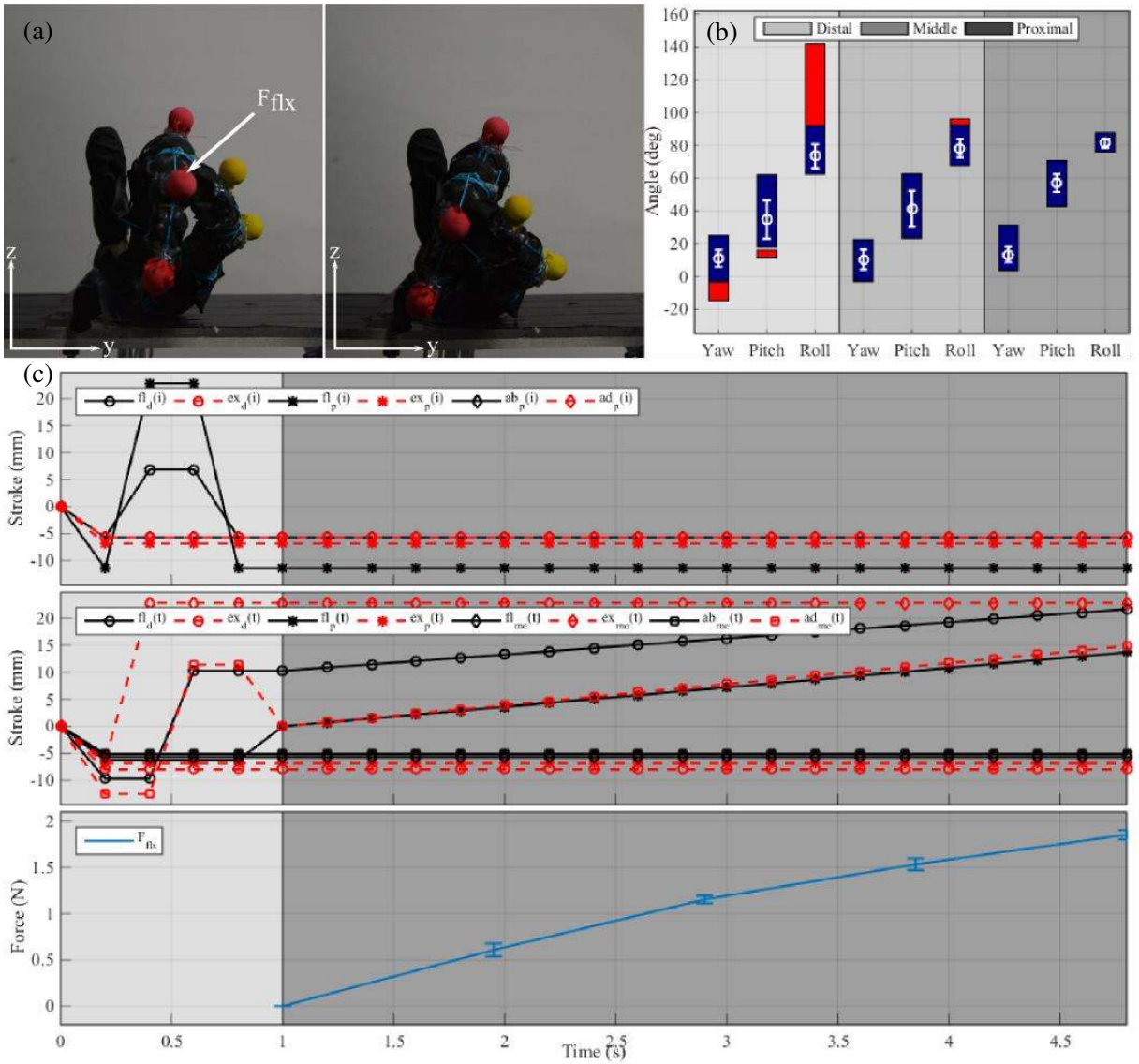

Figure 11. Flexion experiment. The initial (left) and the final (right) poses of fingers are shown with the direction of the pushing F_{flx} force (a). The extension of index finger's range of motion is shown with red bars added to the normal range in figure 7 (b). Top and middle figures are showing the tendon excursions of both fingers in setup (light shade) and action (dark shade) phases. Bottom figure shows the normal force acting on the index finger's tip during action phase (c).

When all three experiments are combined we see an important increase in the range of motions, which show the multi-directional passive compliance of the anthropomorphic joints. The percentage of increase for each phalange is given in table 4.

Table 4. The overall increase in the range of motion of the index finger phalanges.

Phalange	Yaw	Pitch	Roll
Distal	52.2	29.1	244.6
Middle	1.1	0	15.5
Proximal	0	6.2	4.7

3.5. Experiments on Passively Extending Grip

In order to show the adaptation potential of compliant anthropomorphic joints, we perform two additional experiments where we demonstrate extension to the grip size of our robotic hand with two

fingers. In these experiments, we first find the tendon action combinations which will generate a large gap between the tips of the index finger and the thumb. This gap, as we call the grip size, is the distance where the fingers can grab an object without dropping it. Then we place a cylindrical object whose length can be adjusted with a ball screw that can elongate from 8 to 16cm. Similar to the previous experiments, we place a colour marker on the object and the fingers for 3D reconstruction and the analysis of the ranges.

The combinations of the tendon actions show that we can find two configurations for the largest grip size. The former one is what we call the inner grip, is the position where the thumb is adducted towards the middle finger with a curl, and the index finger is extended to straight position being abducted, which can be seen from the leftmost image of figure 12 (a). The object that fits in this gap starts from a length of 10 cm and is extended to 13cm where the fingers can still grip as shown in the pictures of figure 12 (a). Figure 12 (b) shows that the passive compliance of the joints allow the extension of range which generates a larger gripping size with an increase of 30% for this particular finger combination.

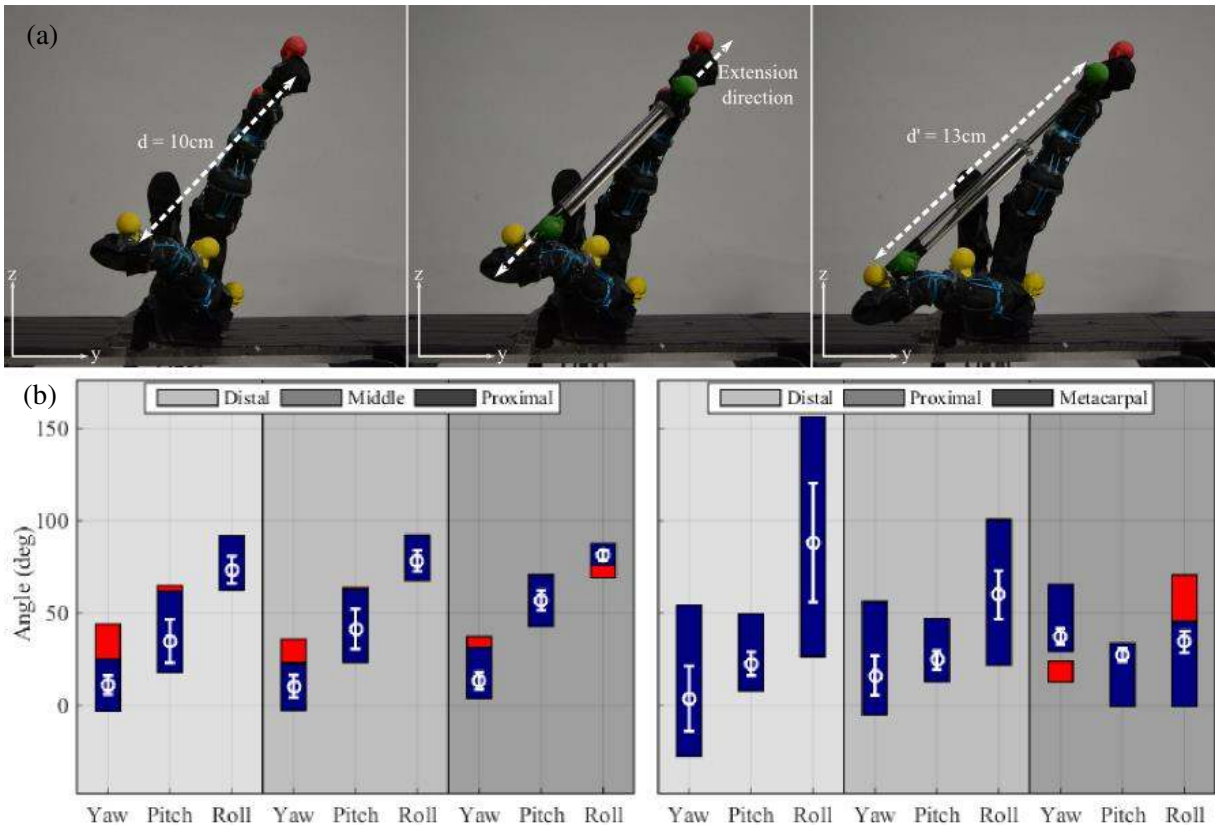

Figure 12. Picture series show the passive extension of the gripping gap from 10 to 13 cm with the extendible object (a). The extension of range of motion during the gripping experiments is shown with red bars (b).

In the other combination, called the outer grip, the thumb is located outside the index finger, extended and abducted, while the index finger is curled with the activation of flexor tendons as shown in figure 13 (a). In this configuration, the grip size is 8 cm and we can extend the object up to 13cm until the fingers cannot grip anymore. The results in figure 13 (b) show that the extension of the joints of both index finger and the thumb allow the increase of grip size with 62.5%.

From the perspective of robotic grasping, these experiments only reflect the adaptation capacity of our compliant jointed fingers as we do not investigate the friction property of the finger tips or the manipulation of the object within the fingers. However, as much as the force closure, the form closure is very important and exploited in compliant grasping [35]. Therefore, in these terms, these

experiments hint the potential of our adaptive fingers to conform to large objects during robotic manipulation which can constitute necessary grasping conditions for form closures.

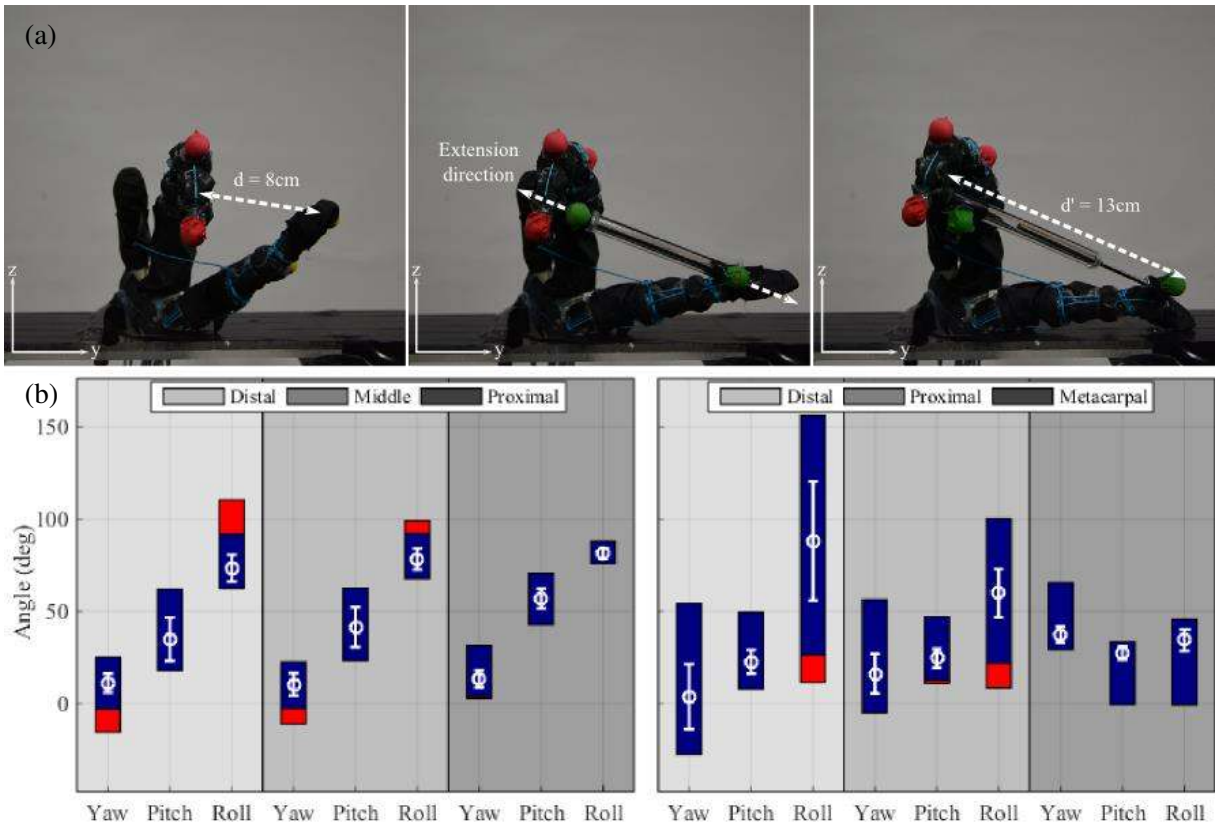

Figure 13. Picture series show the passive extension of the gripping gap between tips of index finger and thumb by placing an extendible stick. In this configuration thumb is abducted and index finger adducted to their possible furthest points within the active range (a). The grip extends from 8 cm to 13 cm with the compliance of joints and their extended range of motion which are shown with red bars(b).

4. Discussion

4.1. Impact of anthropomorphic joint design on finger performance

The main objective of this paper was to establish a design direction towards building anthropomorphic joints which can allow multi-directional compliance while maintaining a strong force exertion and closer actuator-finger posture relation. We believe that such a design can bring the advantages of both ends of anthropomorphic hand design approaches together, making the robotic hands more adaptive, less dependent on active control, stronger in grasping forces and less fragile during interactions with environment.

The first impact of the joint design in this paper becomes clear during the interactions hinted from the normal range of motions in figure 8. The motion range data in this figure show that the range of thumb distal and proximal phalanges actually contain the distal and middle of the index finger. As the base point to calculate these angles is the same for both fingers, these angle ranges can also interpreted as the workspace of fingers. This gives the clue that if two fingers start interacting, the thumb can be used to extend the range of the index finger under certain tendon combinations. Based on this indication, the three experiments show that when the thumb is actuated to push the index finger towards certain locations, its range of motion is extended (up to 245% in the distal roll) clearly.

The main contributor to extension of motion range is the multi-directional compliance provided from the elastic ligaments covering the joints and the geometry of the bone and tendon structures. When the interaction force is applied on the index finger, the joints react and the finger changes its pose

passively to adapt to the stimuli in 3D space. Table 4 summarizes the result of this adaptive motion and shows that it exists in all of three axes for the index finger. In addition to this, Figure 12(b) and 13(b) represent the same passive adaptation for grip extension experiments. Similar to the human hands, such a passive adaptation can only be achieved by an anthropomorphic joint design that integrates different types of elastic materials, which regulates the compliance in multiple directions instead of fixed DOF mechanisms like hinges or gimbals. This compliance can be useful for the development of robotic manipulators which are safer to operate next to humans, or less fragile fingers which can resist unexpected impacts during operation. Additionally, as the gripping experiments show, the deformation of the joint ligaments can generate a larger grasping gap, which can be beneficial for adapting to larger objects in robotic manipulation.

While the elastic ligaments enable the passive compliance, the rigid bones and the non-stretching tendons transfer the actuator torque to force exerted at the finger tips. We notice that in the extension experiments the thumb can exert forces up to 4N as seen in figure 10 (c). This is another indication that the current joint design can make the robotic hands flexible and strong at the same time. The current strength of our fingers is limited with the torque output of the actuators; however this strength can be further increased with using stronger actuators. In addition to this, studies [13] suggest that human tendon arrangement generates a variable moment arm with respect to joint angles which is an important indication on force control for a robotic hand. In our paper, tendon arrangements are primarily chosen to generate the necessary flexion/extension and abduction/adduction motion of the fingers similar to the human hand. Their contribution to the transfer of actuator torque to gripping force is only monitored as a total force at the finger tips during experiments. Even though their influence on the variable moment arm can be a possible future investigation, in the current state of our research we are not implementing a force control which can explore these points.

Additionally, the current design contributes to establishing the relation between actuator and finger posture which is a typical challenge for underactuated systems. Although being composed of 14 tendons that articulate 6 joints with multiple directions of compliance, our experiments shown in figure 8 indicate that the correlation between these two can still be established. This figure shows the influence of each tendon on every phalange's motion axes in means of magnitude and direction. Therefore understanding such a relation can be useful for soft robotic hands from the perspectives of posture control and learning of hand-motor coordination.

4.2. Future Work

The current state of our platform yields sufficient results for the impact of compliant joints on the hand performance in means of adaptation; however we are planning to improve it in different perspectives. The actuators of the system are simple DC gear motors with low torque output (0.22 Nm) that greatly limits the force exertion capacity of our fingers. Studies [20] show that anthropomorphic hand designs with soft elements can still generate sufficient force output with stronger actuators which is a clear indication to explore the actuator influence on our hand design. In addition to a focus on friction forces at the finger tips, this can be exploited to investigate the gripping force and manipulation of objects. Also alternative sensing technologies for load detection and finger pose estimation based on deformable soft materials [36] and design strategies [37] can be implemented on the joints to improve the precision of the system.

An interesting next step would be analysing the relationship between the tendons and their implications on the system with tools like machine learning. As the system consists of 14 tendons, applying machine learning to replicate human hand motions can reveal further behaviours enabled by compliant joints such as coin flipping or finger lock-release. Also the variable moment arm influence from anatomic tendon routing design can be investigated to have a better understanding on the force transmission to finger tips.

We are also planning to assemble a complete hand that can fit with the human hand behaviour replication with learned actions and perform more complicated behaviours and manipulation tasks. A side by side comparison of our complete robot hand with the real human hand can lead to understanding the dexterous capacity of our suggested design. Also the impact resisting capacity of the fingers and joints can be investigated by applying multi-directional impact impulse to see the durability of the design and compared to the human hand and other robot designs which can withstand impacts during operation [38,39].

4.3. Conclusion

In this paper we presented our anthropomorphic joint design that consists of anatomically correct bones, elastic joints and antagonistic tendons to show the principal of multi-directional passive compliance of fingers during interactions. While such an adaption cannot be met with fixed DOF mechanisms widely used in robotic hands, our joints showed noticeable increases of range of motion of the finger phalanges. In order to show the extensions, we use the interactions between the thumb and the index finger, whose great importance in human hand performance is analysed in biology and accepted in robotics field. Our experiments also show that passive compliance of the joints can also increase the grip size of our hand, which has practical uses in robotics field in general; prosthetics and human robot interaction especially. Our choice of the joint design can allow multi-directional passive compliance while being able to exert necessary forces at finger tips and maintain an actuator-finger posture relation, which are the main challenges we addressed to explore the steps for the next generations of anthropomorphic hands.

5. Acknowledgement

This research was supported by the RoboSoft - Coordination Action for Soft Robotics, funded by the European Commission under the Future and Emerging Technologies - (FP7-ICT-2013-C project No 619319).

6. References

[1] Napier J R, Tuttle R and Tuttle R H 1993 *Hands* Princeton University Press.

[2] Pfeifer R and Bongard J 2006 *How the Body Shapes the Way We Think: A New View of Intelligence* MIT Press

[3] Biagiotti L, Lotti F, Melchiorri C and Vassura G 2004 *How far is the human hand? a review on anthropomorphic robotic end-effectors* (DEIS–DIEM, University of Bologna, Bologna)

[4] Controzzi M, Cipriani C and Carrozza M C 2014 Design of artificial hands: A review *The Human Hand as an Inspiration for Robot Hand Development* **95** 219-246

[5] Kapandji I A 1987 *The Physiology of the Joints: Lower Limb* vol 2 Elsevier Health Sciences

[6] Salisbury J K and Craig J J 1982 Articulated hands force control and kinematic issues. *The International Journal of Robotics Research* **1(1)** 4-17

[7] Townsend W 2000 The BarrettHand grasper-programmably flexible part handling and assembly *Industrial Robot: an International Journal* **27(3)** 181-188

[8] Kawasaki H, Komatsu T and Uchiyama K 2002 Dexterous anthropomorphic robot hand with distributed tactile sensor: Gifu hand II *IEEE/ASME Transactions on Mechatronics* **7(3)** 296-303

[9] Bluethmann W, Ambrose R, Diftler M, Askew S, Huber E, Goza M, Rehnmark F, Lovchik C and Magruder D 2003 Robonaut: A robot designed to work with humans in space *Autonomous Robots* **14(2-3)** 179-197

[10] Jacobsen S C, Iversen E K, Knutti D F, Johnson R T and Biggers K B 1986 Design of the Utah/MIT dextrous hand *Proc. IEEE Int. Conf. on Robotics and Automation* 1520-32

[11] Liu H *et al* 2008 Multisensory five-finger dexterous hand: The DLR/HIT Hand II *IEEE/RSJ Int. Conf. on Intelligent Robots and Systems IROS* 3692-97

[12] Shadow Hand 2010 Shadow robot company [Online] http://www.shadowrobot.com/hand/

[13] Deshpande A D, Xu Z, Weghe M J V, Brown B H, Ko J, Chang L Y, Wilkinson D D, Bidic S M and Matsuoka Y 2013 Mechanisms of the anatomically correct testbed hand *IEEE/ASME Transactions on Mechatronics* **18(1)** 238-250

[14] Hirose S and Umetani Y 1978 The development of soft gripper for the versatile robot hand *Mechanism and Machine Theory* **13(3)** 351-359

[15] Catalano M G, Grioli G, Farnioli E, Serio A, Piazza C and Bicchi A 2014 Adaptive synergies for the design and control of the Pisa/IIT SoftHand *The International Journal of Robotics Research* **33(5)** 768-782

[16] Gaiser I *et al* 2008 A new anthropomorphic robotic hand. *IEEE-RAS Int. Conf. on Humanoid Robots* 418-422

[17] Dollar A M and Howe R D 2010 The highly adaptive SDM hand: Design and performance evaluation *The International Journal of Robotics Research* **29(5)** 585-597

[18] Odhner L U *et al* 2014 A compliant, underactuated hand for robust manipulation *The International Journal of Robotics Research* **33(5)** 736-752

[19] Manti M, Hassan T, Passetti G, D'Elia N, Laschi C and Cianchetti M 2015 A Bioinspired soft robotic gripper for adaptable and effective grasping *Soft Robotics* **2(3)** 107-116

[20] Deimel R and Brock O 2014 A novel type of compliant, underactuated robotic hand for dexterous grasping *Robotics: Science and Systems* 1687-92

[21] Deimel R and Brock O 2015 Soft hands for reliable grasping strategies *Soft Robotics* (Springer Berlin Heidelberg) 211-221

[22] Eppner C, Deimel R, Alvarez-Ruiz J, Maertens M and Brock O 2015 Exploitation of environmental constraints in human and robotic grasping *The International Journal of Robotics Research* **34(7)** 1021-1038

[23] Pfeifer R, Iida F and Lungarella M 2014 Cognition from the bottom up: on biological inspiration, body morphology, and soft materials *Trends in Cognitive Sciences* **18(8)** 404-413

[24] Xu Z, Kumar V, Matsuoka Y and Todorov E 2012 Design of an anthropomorphic robotic finger system with biomimetic artificial joints. *IEEE RAS & EMBS Int. Conf. Biomedical Robotics and Biomechatronics BioRob* 568-574

[25] Cutkosky M R 1989 On grasp choice, grasp models, and the design of hands for manufacturing tasks *IEEE Transactions on Robotics and Automation* **5(3)** 269-279

[26] Chao E Y 1989 *Biomechanics of the Hand: a Basic Research Study* World Scientific

[27] Katarincic J A 2001 Thumb kinematics and their relevance to function *Hand Clinics* **17(2)** 169-174

[28] Minami A, An K N, Cooney W P, Linscheid R L and Chao E Y S 1984 Ligamentous Structures of the metacarpophalangeal joint: a quantitative anatomic study 1984 *Journal of Orthopedic Research* **1(4)** 361-38

[29] Ralphs J R and Benjamin M 1994 The joint capsule: structure, composition, ageing and disease *Journal of Anatomy* **184(3)** 503-509

[30] Wang L and Iida F 2012 Physical connection and disconnection control based on hot melt adhesives *IEEE/ASME Transactions on Mechatronics* **18(4)** 1397-1409

[31] MATLAB and Computer Vision System Toolbox Release 2014b The MathWorks Inc. (Natick-Massachusetts United States)

[32] Hartley R and Zisserman A 2003 *Multiple View Geometry in Computer Vision* Cambridge University Press

[33] An K N, Ueba Y, Chao E Y, Cooney W P and Linscheid R L 1983 Tendon excursion and moment arm of index finger muscles *Journal of Biomechanics* **16(6)** 419-425

[34] Smutz W P, Kongsayreepong A, Hughes R E, Niebur G, Cooney W P and An K N 1998 Mechanical advantage of the thumb muscles *Journal of Biomechanics* **31(6)** 565-670

[35] Markenscoff X, Ni L and Papadimitriou C H 1990 The geometry of grasping *The International Journal of Robotics Research* **9(1)** 61-74

[36] Culha U, Nurzaman S G, Clemens F and Iida F 2014 SVAS^3: Strain vector aided sensorization of soft structures *Sensors* **14(7)** 12748-70

[37] Nurzaman S G, Culha U, Brodbeck L, Wang L and Iida F 2013 Active sensing system with in situ adjustable sensor morphology *PloS One* **8(12)** e84090

[38] Grebenstein M *et al* 2011 The DLR hand arm system *Proc. IEEE Int. Conf. on Robotics and Automation* 3175-82

[39] Seok S, Onal C D, Wood R, Rus D and Kim S 2010 Peristaltic locomotion with antagonistic actuators in soft robotics *Proc. IEEE Int. Conf. on Robotics and Automation* 1228-33